

ARTICLE OPEN



More water-soluble brown carbon after the residential “coal-to-gas” conversion measure in urban Beijing

Wei Yuan^{1,2}, Ru-Jin Huang^{1,2✉}, Jincan Shen³, Kai Wang⁴, Lu Yang^{1,2}, Ting Wang¹, Yuquan Gong^{1,2}, Wenjuan Cao¹, Jie Guo¹, Haiyan Ni¹, Jing Duan¹ and Thorsten Hoffmann⁵

The implementation of air pollution reduction measures has significantly reduced the concentration of atmospheric fine particles (PM_{2.5}) in Beijing, among which the “coal-to-gas” conversion measures may play a crucial role. However, the effect of this conversion measure on brown carbon (BrC) is not well known. Here, the chemical composition of BrC in humic-like fraction (HULIS-BrC) and water-insoluble fraction (WI-BrC) were characterized for ambient PM_{2.5} samples collected in Beijing before and after the “coal-to-gas” conversion measure. After the conversion measure, the number of HULIS-BrC compounds increased by ~14%, while the number of WI-BrC compounds decreased by ~8%. The intensity of over 90% of HULIS-BrC compounds also increased after the conversion measure, and correspondingly the O/C ratios of CHO and CHON compounds in HULIS-BrC fraction generally increased with the increase of intensity ratios after/before the conversion measure, indicating that there were more water-soluble highly oxygenated BrC compounds after “coal-to-gas” conversion measure. On the contrary, the intensity of more than 80% of WI-BrC compounds decreased after the conversion measure, and the O/C ratios of CHO and CHON compounds in WI-BrC fraction generally decreased with the decrease of intensity ratios after/before the conversion measure, indicating that after the “coal-to-gas” conversion measure the water-insoluble low oxygenated BrC compounds decreased. This work sheds light on the differences in the chemical composition of BrC between before and after the “coal-to-gas” conversion measure and suggests that future studies on the residential coal combustion BrC and secondary BrC deserve further exploration.

npj Climate and Atmospheric Science (2023)6:20; <https://doi.org/10.1038/s41612-023-00355-w>

INTRODUCTION

Haze pollution with a high concentration of fine particle matter (PM_{2.5}) pollution is a notable environmental problem in China, especially during the wintertime heating period, leading to negative effects on air quality and public health^{1–4} as well as the potential impact on climate^{5,6}. To mitigate air pollution, a variety of legislative actions have been applied from the central to local governments, including the “Air Pollution Prevention and Control Action Plan” implemented in 2013, the “Air Pollution Prevention and Control Law” established in 2016, and some regulatory measures, e.g., the “odd-even vehicular ban” and “staggered-peak production” in many cities. With these efforts, the air quality in North China has strikingly improved over the past years, with the annual average PM_{2.5} concentration reducing from 86 $\mu\text{g m}^{-3}$ in 2013 to 37 $\mu\text{g m}^{-3}$ in 2021. Nevertheless, haze pollution still occurred less frequently in wintertime North China, leaving a question about the culprit.

In recent years, there has been mounting evidence suggesting that residential coal combustion is a major emission source responsible for wintertime haze pollution in North China^{1,7–12}. For example, direct emissions from residential coal combustion were found to contribute 25% of organic aerosol (OA) in PM₁ during extremely polluted days in winter 2014 in Shijiazhuang⁹ and 19% of OA in PM₁ during high pollution days in winter 2014 in Beijing¹¹. A residential “coal-to-gas” conversion measure was therefore initiated for the region of Beijing–Tianjin–Hebei and the surrounding area, which requires the replacement of coal with gas

for residential heating and cooking by the end of 2018. Consequently, coal consumption for heating in Beijing decreased by over 70%, from 3.47 million tons in 2015 to 0.97 million tons in 2019 (<http://tjj.beijing.gov.cn/>), while the concentration of PM_{2.5} decreased from 84.0 $\mu\text{g m}^{-3}$ in 2015 to 47.9 $\mu\text{g m}^{-3}$ in 2019 in wintertime Beijing (<http://sthjj.beijing.gov.cn/>). This may affect the light absorption of OA, i.e., the light-absorbing OA fraction, which is also known as brown carbon (BrC), and thus affect the atmospheric photochemical reactions and radiative forcing^{12–16}, because residential coal combustion has recently been recognized as an important BrC source in China, especially during the heating season^{17–19}. As the light absorption properties of BrC is determined by its chemical composition, the residential “coal-to-gas” conversion measure provides a unique scientific platform to gain insights into how the conversion measure affects the BrC chemical composition.

In this study, we present the detailed chemical characterization of different BrC fractions in PM_{2.5} samples collected in urban Beijing before and after the residential “coal-to-gas” conversion measure, with a high-performance liquid chromatograph (HPLC) coupled with a photodiode array (PDA) and a high-resolution Orbitrap mass spectrometer (HRMS) in both negative (ESI[–]) and positive mode electrospray ionization (ESI⁺). The differences in chromophoric number, intensity, and oxidation status for humic-like BrC fraction (HULIS-BrC) and water-insoluble BrC fraction (WI-BrC) are discussed.

¹State Key Laboratory of Loess and Quaternary Geology, Center for Excellence in Quaternary Science and Global Change, Institute of Earth Environment, Chinese Academy of Sciences, Xi'an 710061, China. ²University of Chinese Academy of Sciences, Beijing 100049, China. ³Key Laboratory of Detection Technology R&D on Food Safety, Food Inspection and Quarantine Technology Center of Shenzhen Customs, Shenzhen 518045, China. ⁴Key Laboratory of Plant-Soil Interactions of MOE, College of Resources and Environmental Sciences, National Academy of Agriculture Green Development, China Agricultural University, Beijing 100193, China. ⁵Department of Chemistry, Johannes Gutenberg University of Mainz, Duesbergweg 10-14, 55128 Mainz, Germany. ✉email: rujin.huang@ieecas.cn

Table 1. Number of chromophores in each compound category of HULIS-BrC and WI-BrC before (2015) and after (2019) the “coal-to-gas” conversion measure.

	2015 HULIS	2019 HULIS	2015 WISOC	2019 WISOC
CH (+)			564	512
CHO (−)	1970	2194	793	711
CHO (+)	1129	1362	1758	1699
CHN (+)	603	643	1811	1587
CHON (−)	2209	2499	1281	1101
CHON (+)	3643	4175	4881	4575
S-containing (−)	109	117	31	29
S-containing (+)	45	42	31	25
BrC ESI (−)	4288	4810	2105	1841
BrC ESI (+)	5420	6222	9045	8398

RESULTS

General characteristics of BrC fraction

The identified formulas are classified into five major compound categories, including CH, CHO, CHN, CHON, and S-containing (CHOS and CHONS), based on their elemental composition. CHO refers to compounds that contain carbon, hydrogen, and oxygen elements. Other compound categories are defined analogously. Supplementary Fig. 1 shows the plots of DBE versus the number of C atoms for all assigned formulas in HULIS and WISOC fractions before (2015) and after (2019) the “coal-to-gas” conversion measure, along with the reference boundary line characteristics of fullerene-like hydrocarbons with $\text{DBE} = 0.9 \times \text{C}^{20,21}$, cata-PAHs with $\text{DBE} = 0.75 \times \text{C} - 0.5^{20,22}$, and linear polyenes $\text{C}_x\text{H}_{x+2}^{20,22}$. The chromophores of BrC have efficient light absorption in UV–vis wavelengths, which requires uninterrupted conjugation across a significant part of the molecular structure. Therefore, compounds with a DBE/C ratio greater than that of polyenes are potential BrC chromophores (see the shaded area in Supplementary Fig. 1)^{20,23}. As shown in Table 1, before and after the measure, a total of 9708 and 11,032 BrC chromophores were detected in the HULIS fraction, while 11,150 and 10,239 BrC chromophores in WISOC fraction, respectively.

Figure 1 shows the number and intensity of different chromophore categories in HULIS-BrC and WI-BrC fractions before and after the “coal-to-gas” conversion measure. In the HULIS-BrC fraction, CHON chromophores have the largest contribution in number (>50%) before and after the measure, followed by CHO (~32%), CHN (~6%), and S-containing (~1.5%) chromophores (Supplementary Fig. 2). For CHON chromophores in HULIS-BrC fraction, more were detected in ESI+ mode than in ESI−, and for CHO chromophores, more were identified in ESI− mode. This result is in line with a previous study of HULIS in the Pearl River Delta Region, China, by Lin et al.²⁴. Unlike the number distribution, the intensity of CHON and CHO chromophores were both higher in ESI− than in ESI+ mode. In the WI-BrC fraction, CHON chromophores also have the largest contribution in number (>50%) before and after the measure, followed by CHO (~23%), CHN (~16%), CH (~5%), and S-containing (~0.5%) chromophores (Supplementary Fig. 2). Different from the HULIS-BrC fraction, the number and intensity of different chromophore categories in WI-BrC fraction are both higher in ESI+ than in ESI− mode. The differences in chromophore number and intensity between HULIS-BrC and WI-BrC can be ascribed to the difference in chromophore composition, and the differences in chromophore composition of HULIS-BrC or WI-BrC between ESI− and ESI+ is mainly due to the different ionization mechanisms^{24,25}.

In the HULIS-BrC fraction, the number and intensity of CHON, CHO, CHN, and S-containing chromophores were generally higher

after the “coal-to-gas” conversion measure than before the measure (increased by about 14%, 15%, 7%, and 3% in number and 80%, 81%, 24% and 51% in intensity for CHON, CHO, CHN and S-containing chromophores, respectively). However, in the WI-BrC fraction, the number and intensity of CHON, CHO, CHN, CH, and S-containing chromophores were generally lower after the measure than before the measure (decreased about 8%, 6%, 12%, 9%, and 13% in number and 34%, 35%, 44%, 52%, and 19% in intensity for CHON, CHO, CHN, CH, and S-containing chromophores, respectively) (Supplementary Fig. 3). These results indicate that after the “coal-to-gas” conversion measure the HULIS-BrC chromophores increased while the WI-BrC chromophores decreased, which could provide a guide for future study on the influences of the measure on optical properties and radiative forcing of atmospheric BrC.

Supplementary Figure 4 shows the reconstructed mass spectra of HULIS-BrC and WI-BrC chromophores before and after the “coal-to-gas” conversion measure, which show obvious differences. It can be seen that after the “coal-to-gas” conversion measure, the intensity of some chromophores increased while others decreased. For example, in the WI-BrC fraction assigned in ESI+ mode, the total intensity was higher for CHN+ chromophores than CHO+ chromophores before the measure, while the total intensity of CHO+ chromophores was similar to that of CHN+ chromophores after the measure. The differences in mass spectra of BrC fractions before and after the “coal-to-gas” conversion measure indicate that the change in emission sources and, thus, atmospheric processing alter the chromophore composition of atmospheric BrC. In the following sections, the differences for all the five chromophore categories in BrC fractions before and after the “coal-to-gas” conversion measure are discussed.

CHO chromophores

CHO compounds are a class of common compounds identified in atmospheric organic aerosol^{26–29}, which could be from both primary emissions^{30,31} and secondary formation^{32,33}. A total of 3099 and 3556 CHO chromophores were assigned in HULIS-BrC fraction before and after the “coal-to-gas” measure, respectively, and correspondingly 2551 and 2410 were assigned in WI-BrC fraction (Fig. 1). Figure 2 shows that van Krevelen diagram for CHO chromophores in HULIS-BrC and WI-BrC fractions in ESI− mode (CHO−). The peak intensity-weighted average molecular formulas (MF_{avg}) for CHO− chromophores in HULIS-BrC and WI-BrC were $\text{C}_{9.85}\text{H}_{8.21}\text{O}_{3.43}$ and $\text{C}_{11.56}\text{H}_{8.81}\text{O}_{2.93}$, respectively, before “coal-to-gas” conversion measure, and $\text{C}_{9.66}\text{H}_{8.05}\text{O}_{3.60}$ and $\text{C}_{11.09}\text{H}_{8.56}\text{O}_{3.04}$, respectively, after the measure (Supplementary Table 1). The CHO− chromophores in HULIS-BrC fraction before and after the measure were dominated by monocyclic aromatics ($2.5 \leq \text{Xc} < 2.7$)

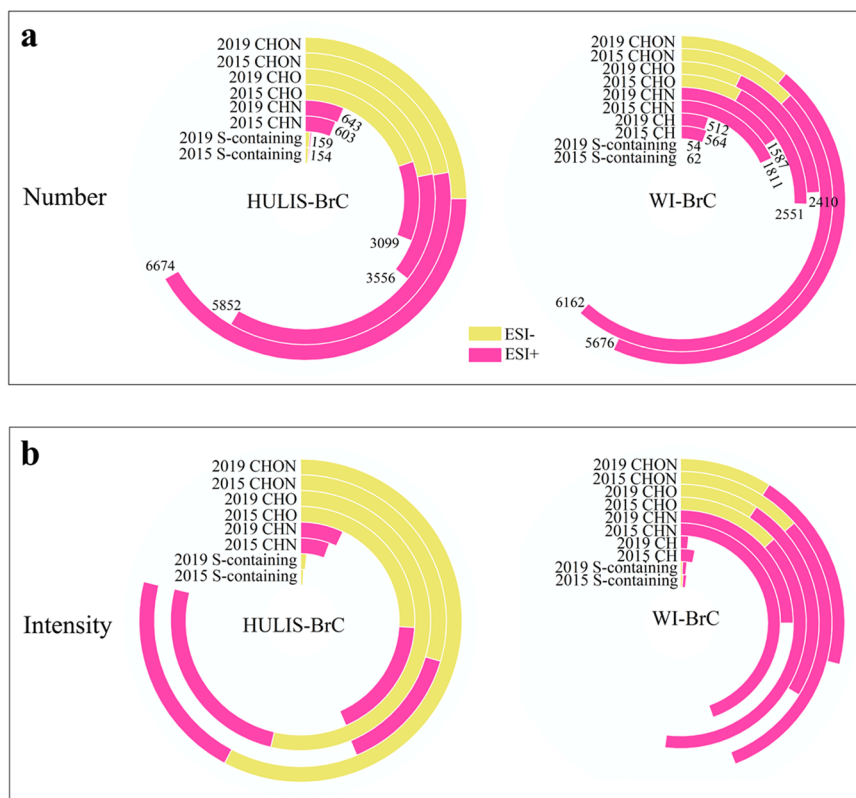


Fig. 1 Chromophores in each compound category of HULIS-BrC and WI-BrC fractions before (2015) and after (2019) the “coal-to-gas” conversion measure. **a** Number and **b** intensity of chromophores.

(44% and 45% in terms of peak intensity, respectively) and polycyclic aromatics ($2.7 \leq X_c$) (44% and 42% in terms of peak intensity, respectively) (Fig. 2a, b). The corresponding intensity of most CHO- chromophores in the HULIS-BrC fraction was higher after the measure than before the measure, and the O/C ratios generally increased with the increase of intensity ratios after/before the measure (Fig. 2e). For example, the average O/C ratios of CHO- chromophores in HULIS-BrC fraction was non-aromatics ($X_c < 2.5$) (0.49) > monocyclic aromatics (0.30) > polycyclic aromatics (0.24), and the average intensity ratios of after/before the measure was also non-aromatics (2.6 times) > monocyclic aromatics (2.1 times) > polycyclic aromatics (1.9 times). Besides, only 5 extra CHO- chromophores in the HULIS-BrC fraction were identified before the measure, but none after the measure, and their O/C ratios were all less than 0.3 (0.18 on average). In comparison, 229 extra CHO- chromophores in the HULIS-BrC fraction were identified after the measure but none before the measure, with the O/C ratio of 0.34 on average. The peak intensity-weighted O/C ratio (O/C_{avg}) of CHO- chromophores in HULIS-BrC fraction were 0.36 and 0.39 before and after the “coal-to-gas” conversion measure, respectively (Supplementary Table 1). These results indicate that more highly oxygenated CHO- chromophores existed in the HULIS-BrC fraction after the “coal-to-gas” conversion measure than before the measure. These increased CHO- chromophores in HULIS-BrC could possibly be explained by the increase of secondary BrC^{34,35}. Although the concentrations of $PM_{2.5}$ and other pollutants (e.g. CO and NO_2) were indeed decreased in Beijing after the “coal-to-gas” conversion measure (52 and $38 \mu g m^{-3}$ of $PM_{2.5}$ and NO_2 , respectively, $0.8 mg m^{-3}$ of CO) compared with those before measure (84 and $52 \mu g m^{-3}$ of $PM_{2.5}$ and NO_2 , respectively, $1.4 mg m^{-3}$ of CO), the concentration of O_3 (60 and $67 \mu g m^{-3}$ before and after “coal-to-gas” conversion measure, respectively) (<http://sthjj.beijing.gov.cn/>) was not decreased, which is one of the major sources of OH radicals.

Siemens et al.³⁵ reported the formation of secondary CHO- chromophores from the photooxidation of anthropogenic aromatic volatile organic compound (VOC).

The CHO- chromophores in WI-BrC fraction before and after the “coal-to-gas” conversion measure were dominated by polycyclic aromatics (47% and 46% in terms of peak intensity, respectively) and monocyclic aromatics (40% and 40%, respectively) (Fig. 2c, d). In contrast to CHO- chromophores in the HULIS-BrC fraction, the corresponding intensity of most CHO- chromophores in the WI-BrC fraction was higher before the measure than after the measure, and the O/C ratios of CHO- in WI-BrC fraction generally increased with the decrease of intensity ratios of before/after the measure (Fig. 2f). For example, the average O/C ratios of CHO- chromophores in WI-BrC fraction was non-aromatics (0.48) > monocyclic aromatics (0.28) > polycyclic aromatics (0.17), and the average intensity ratios of before/after the measure were polycyclic aromatics (1.8 times) > monocyclic aromatics (1.5 times) > non-aromatics (1.2 times). There were 97 extra CHO- chromophores in the WI-BrC fraction identified before the measure but none after the measure, with the average O/C ratio of 0.16, while only 15 extra CHO- chromophores in WI-BrC fraction were identified after the measure but none before the measure, with the average O/C ratios of 0.44. The O/C_{avg} of CHO- chromophores in WI-BrC fraction were 0.29 and 0.31, respectively, before and after the “coal-to-gas” conversion measure (Supplementary Table 1). These results indicate that less low-oxygenated CHO- chromophores existed in WI-BrC fraction after the “coal-to-gas” conversion measure than before the measure, which may be related to the reduction of primary emissions (e.g. coal and biomass burning)^{36,37}.

The CHO + chromophores in HULIS-BrC and WI-BrC fractions have similar changing characteristics with CHO- chromophores in HULIS-BrC and WI-BrC fractions before and after the “coal-to-gas” measure (Supplementary Figure 5). These results indicate that

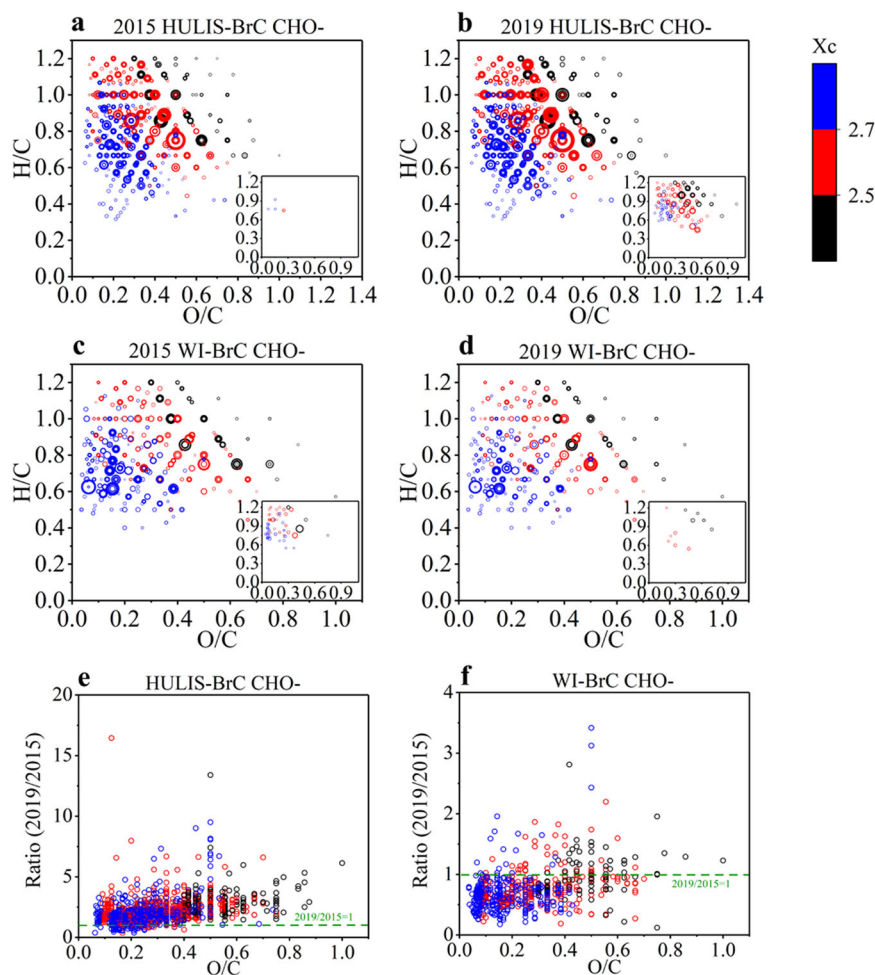


Fig. 2 Characteristics of CHO chromophores assigned in ESI-mode before (2015) and after (2019) the “coal-to-gas” conversion measure. **a, b** Van Krevelen diagram for CHO– chromophores in HULIS-BrC fraction. **c, d** Similar to (**a, b**), but in WI-BrC fraction. **e** Corresponding intensity ratios of after/before (2019/2015) the measure of CHO– chromophores in HULIS-BrC fraction. **f** Similar to (**e**), but in the WI-BrC fraction. The area of the circles is proportional to the fourth root of the intensity of individual chromophores, and the color bar denotes the aromaticity equivalent (black with $X_c < 2.5$, red with $2.5 \leq X_c < 2.7$, and blue with $X_c \geq 2.7$). The insert plot represents the chromophores identified only before or after the measure.

after the “coal-to-gas” conversion measure, the water-insoluble CHO chromophores decreased, while the water-soluble CHO chromophores increased.

CHON chromophores

CHON chromophores have the highest number in BrC fractions before and after the “coal-to-gas” conversion measure. A total of 5852 and 6674 CHON chromophores were assigned in the HULIS-BrC fraction before and after the measure, respectively, while 6162 and 5676 were assigned in the WI-BrC fraction correspondingly. The MF_{avg} for CHON– and CHON+ chromophores in HULIS-BrC were $C_{7.67}H_{7.21}O_{3.50}N_{1.11}$ and $C_{10.21}H_{9.96}O_{1.95}N_{1.30}$, respectively, before “coal-to-gas” conversion measure, and $C_{7.62}H_{7.06}O_{3.59}N_{1.18}$ and $C_{10.13}H_{10.12}O_{2.24}N_{1.38}$, respectively, after the measure. The MF_{avg} for CHON– and CHON+ chromophores in WI-BrC were $C_{8.80}H_{8.81}O_{3.47}N_{1.10}$ and $C_{13.06}H_{12.14}O_{1.78}N_{1.35}$, respectively, before “coal-to-gas” conversion measure, and $C_{8.56}H_{8.33}O_{3.62}N_{1.21}$ and $C_{12.52}H_{12.12}O_{1.95}N_{1.44}$, respectively, after the measure (Supplementary Table 1). These results suggest that CHON chromophores in BrC after the “coal-to-gas” conversion measure contain more O and N atoms on average than those before the measure. Figure 3 shows the van Krevelen diagram for CHON chromophores in HULIS-BrC and WI-BrC fractions assigned in ESI– mode.

The CHON– chromophores in the HULIS-BrC fraction were dominated by monocyclic aromatics (59% and 61% in terms of peak intensity before and after the measure, respectively) (Fig. 3a, b), and the corresponding intensity of most of CHON– chromophores in HULIS-BrC fraction was higher after the measure than before the measure (Supplementary Figure 6a). We further classified CHON– chromophores in HULIS-BrC fraction into different subgroups according to their O/N ratios (Fig. 4a, b); it can be seen that most CHON– chromophores in HULIS-BrC fraction (56% and 56% in terms of formula numbers before and after the measure, respectively) have $O/N \geq 3$, which may contain one nitro ($-\text{NO}_2$) or nitrooxy ($-\text{ONO}_2$) group. Further, more than 35% of CHON– chromophores in the HULIS-BrC fraction have $O/N \geq 4$, which may indicate the presence of further oxygenated functional groups, such as a hydroxyl group ($-\text{OH}$) or a carbonyl group ($\text{C}=\text{O}$)^{24,38}. There were 12 CHON– chromophores in the HULIS-BrC fraction identified only before the measure but none after the measure and 75% of them have $O/N < 3$. On the contrary, 302 CHON– chromophores in the HULIS-BrC fraction were assigned only after the measure but none before the measure and over 50% of them have $O/N \geq 3$. These results indicate that most of these increased CHON– chromophores in HULIS-BrC fraction after the “coal-to-gas” conversion measure may be nitroaromatic and organonitrate compounds, which could be

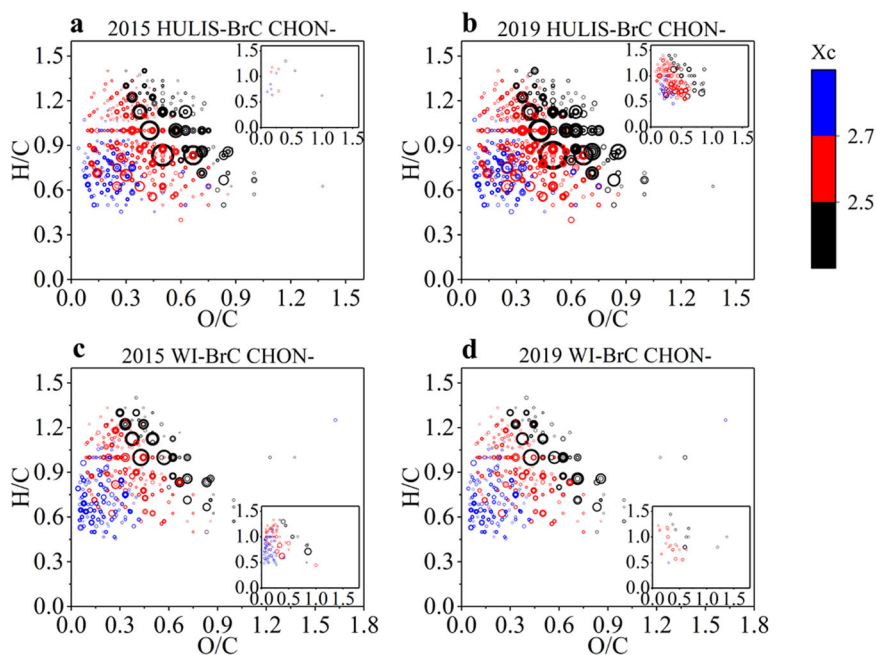


Fig. 3 Van Krevelen diagram for CHON chromophores assigned in ESI- mode before (2015) and after (2019) the “coal-to-gas” conversion measure. CHON- chromophores in **a, b** HULIS-BrC and **c, d** WI-BrC fractions. The area of the circles is proportional to the fourth root of the intensity of individual chromophores, and the insert plot represents the chromophores identified only before or after the measure. The color bar denotes the aromaticity equivalent (black with $X_c < 2.5$, red with $2.5 \leq X_c < 2.7$, and blue with $X_c \geq 2.7$).

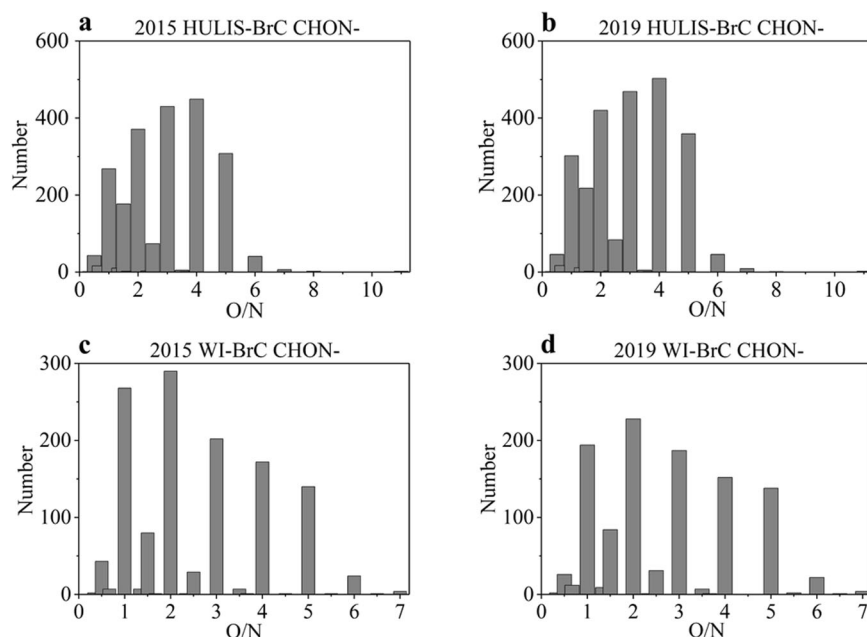


Fig. 4 Number of different CHON- chromophore subgroups classified according to O/N ratios in their formulas. **a, c** Number of different CHON- chromophore subgroups in HULIS-BrC and WI-BrC fractions before (2015) the “coal-to-gas” conversion measure. **b, d** Similar to **(a, c)**, but after (2019) the “coal-to-gas” conversion measure.

from secondary formation^{24,39–42}. Wang et al.⁴² reported the formation of CHON- chromophores from oxidation of anthropogenic VOCs in the presence of NO_x.

The CHON- chromophores in WI-BrC fraction before and after the “coal-to-gas” conversion measure were also predominated by monocyclic aromatics (53% and 54% in terms of peak intensity, respectively) (Fig. 3c, d). Different from CHON- chromophores in the HULIS-BrC fraction, the corresponding intensity of a majority of CHON- chromophores in the WI-BrC fraction was higher before

the measure than after the measure (Supplementary Fig. 6b). CHON- chromophores with O/N ratio of 2 dominated the CHON- chromophores in WI-BrC fraction and most CHON- chromophores in WI-BrC fraction have O/N < 3 (57% and 53% in terms of formula numbers before and after the measure, respectively) (Fig. 4c, d), suggesting they may contain reduced nitrogen function groups (e.g., amines)^{24,38}. There were 223 CHON- chromophores in the WI-BrC fraction assigned only before the measure, and none after the measure, and about 79% of them have O/N < 3, while only 43

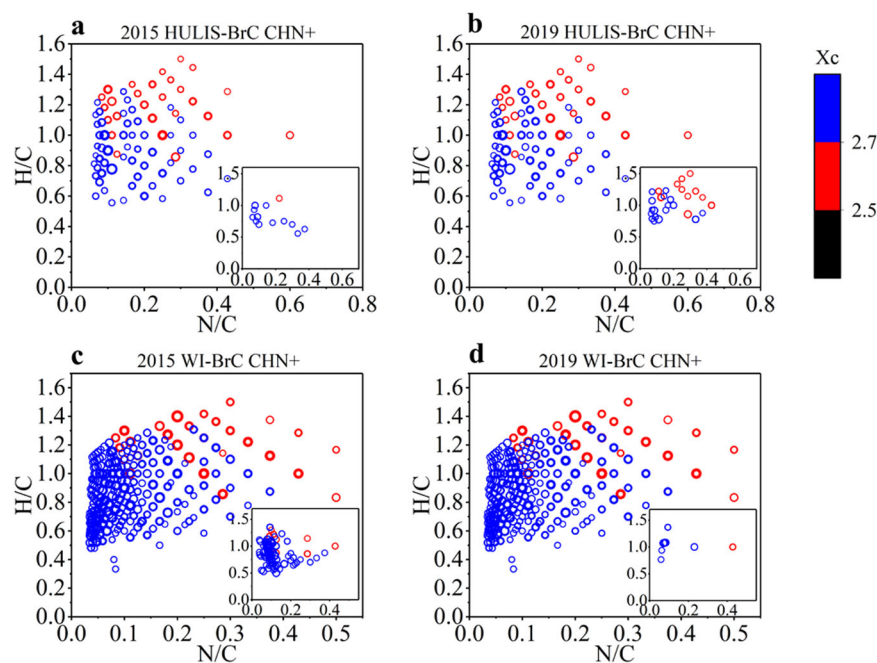


Fig. 5 Van Krevelen diagram for CHN+ chromophores. **a, c** Van Krevelen diagram for CHN+ chromophores in HULIS-BrC and WI-BrC fractions before (2015) the “coal-to-gas” conversion measure. **b, d** Similar to (**a, c**), but after (2019) the “coal-to-gas” conversion measure. The area of the circles is proportional to the fourth root of the intensity of individual chromophores, and the color bar denotes the aromaticity equivalent (black with $X_c < 2.5$, red with $2.5 \leq X_c < 2.7$, and blue with $X_c \geq 2.7$). The insert plot represents the chromophores identified only before or after the measure.

CHON– chromophores in the WI-BrC fraction were assigned after the measure, but none before the measure and about 81% of them have $O/N < 3$. These results indicate that after the “coal-to-gas” conversion measure, CHON– chromophores with less-oxidized structures in WI-BrC fraction decreased a lot, which may be due to the decrease of combustion emissions^{36,43,44}.

CHON+ chromophores in HULIS-BrC fraction before and after the “coal-to-gas” conversion measure have similar characteristics with CHON– chromophores in HULIS-BrC fraction, which were also dominated by monocyclic aromatics (55% and 53% in terms of peak intensity, respectively) (Supplementary Figure 7a, b). The corresponding intensity of most CHON+ chromophores in the HULIS-BrC fraction was also higher after the measure than before the measure (Supplementary Fig. 8a), and more extra CHON+ chromophores in HULIS-BrC fraction were assigned only after the measure (Supplementary Figure 7a, b). The chromophore composition of CHON+ was different from CHON– in the HULIS-BrC fraction, which could be due to the difference in ionization efficiency between the positive and negative modes^{24,25}. A majority of CHON+ chromophores in HULIS-BrC fraction have $O/N < 3$ (69% and 68% in terms of formula numbers before and after the measure, respectively) (Supplementary Fig. 9a, b), suggesting they could contain reduced nitrogen function groups^{24,38}. Different from CHON+ chromophores in the HULIS-BrC fraction, the CHON+ chromophores in the WI-BrC fraction before and after the measure was mainly composed of polycyclic aromatics (47% and 44% in terms of peak intensity, respectively) and monocyclic aromatics (34% and 34%, respectively) (Supplementary Fig. 7c, d). Like the CHON– chromophores in the WI-BrC fraction, most CHON+ chromophores in the WI-BrC fraction also have $O/N < 3$ (62% and 60% in terms of formula numbers before and after the measure, respectively) (Supplementary Figure 9c, d). The corresponding intensity of most CHON+ chromophores in the WI-BrC fraction was higher before the measure than after the measure (Supplementary Fig. 8b), and more extra CHON+ chromophores were assigned in WI-BrC fraction only before the measure (Supplementary Fig. 7c, d). These results suggest that

there was a large number of CHON+ chromophores with low oxidation degrees in both water-soluble and water-insoluble BrC, and after the “coal-to-gas” conversion measure, the water-soluble CHON+ chromophores increased, while the water-insoluble CHON+ chromophores decreased.

CHN+ chromophores

In ESI+ mode, a total of 603 and 643 CHN chromophores in HULIS-BrC fraction were assigned before and after the “coal-to-gas” conversion measure, respectively (6.2% and 5.8% in terms of formula numbers, respectively), and 1811 (16.2%) and 1587 (15.5%) were identified in WI-BrC fraction, respectively. The CHN+ chromophores assigned in this study were composed of aromatics ($X_c \geq 2.5$), implying a high degree of aromaticity. The van Krevelen diagram of CHN+ chromophores in HULIS-BrC and WI-BrC fractions before and after the “coal-to-gas” measure is shown in Fig. 5. The CHN+ chromophores in HULIS-BrC fraction were mainly composed of polycyclic aromatics (69% and 67% in terms of peak intensity before and after the measure, respectively) (Fig. 5a, b). The corresponding intensity of most CHN+ in the HULIS-BrC fraction was higher after the measure than before the measure (Supplementary Fig. 10a), and more extra CHN+ chromophores in the HULIS-BrC fraction were assigned only after the measure. The CHN+ chromophores in the WI-BrC fraction were also mainly composed of polycyclic aromatics (86% and 85% in terms of peak intensity before and after the measure, respectively) (Fig. 5c, d). However, the corresponding intensity of a majority of CHN+ chromophores in the WI-BrC fraction was higher before the measure than after the measure (Supplementary Fig. 10b), and more extra CHN+ chromophores in WI-BrC fractions were assigned only before the measure. It should be noted that in the HULIS-BrC fraction before and after the “coal-to-gas” measure, the CHN+ chromophores generally have carbon atoms < 15 and DBE 5–12 (Supplementary Fig. 11a, b), which were suggested to be alkaloids⁴⁴, and in WI-BrC fraction, there were a large number of CHN+ chromophores with carbon atoms > 15 and DBE 12–24

(Supplementary Fig. 11c, d), which were assigned to fused aromatic structures and N-heterocyclic rings^{24,44}. According to previous studies, the increased CHN+ chromophores in the HULIS-BrC fraction may be formed from the photooxidation of aromatic hydrocarbons^{45,46}, and the decreased CHN+ chromophores in WI-BrC fraction could be due to the reduction of fossil fuel combustion (especially coal combustion)^{38,47,48}.

S-containing chromophores

A total of 154 and 159 S-containing chromophores were identified in HULIS-BrC fraction before and after the “coal-to-gas” measure, respectively, while they were 62 and 54 in the WI-BrC fraction. The S-containing chromophores include CHOS and CHONS. For CHOS chromophores, they were dominated by aliphatic compounds ($X_c < 2.5$), and most of them were detected in the HULIS-BrC fraction in ESI⁻ mode. The majority of CHOS chromophores have O/S ratios of 4–11 (Supplementary Fig. 12), indicating the possibility of at least one $-OSO_3H$ functional group and thus a possible classification to organosulfates (OSs)^{29,38}. The corresponding intensity of most CHOS chromophores in BrC was higher after the “coal-to-gas” conversion measure (7.0×10^7 in total) than before the measure (5.5×10^7 in total) (Supplementary Fig. 13), which could be formed by secondary reactions of primary precursors^{24,38,49–51}. For CHONS chromophores, in the HULIS-BrC fraction, most of them were identified in ESI⁻ mode, while in the WI-BrC fraction, a majority of them were measured in ESI⁺ mode (Supplementary Fig. 14). Like CHOS chromophores, more CHONS chromophores were assigned in HULIS-BrC fraction than in WI-BrC fraction. More than 70% of CHONS chromophores in HULIS-BrC and WI-BrC fractions have O atoms < 7 , suggesting that they may contain reduced S (e.g., aromatic S-containing compounds) or reduced N functional groups (e.g., nitrile)³⁶. Besides, before and after the measure, about 24% and 26% of CHONS chromophores in HULIS-BrC fraction and about 21% and 20% of CHONS chromophores in WI-BrC fraction were assigned with O atoms ≥ 7 , suggesting they may contain one $-OSO_3H$ and one $-NO_3$ functional group and they are likely nitrooxy-organosulfates^{27,29,36,38}, which can be formed by the photochemical oxidation of VOCs under high NO_x condition^{49,52}. Similar to CHOS chromophores, the corresponding intensity of most CHONS chromophores in BrC was also higher after the “coal-to-gas” conversion measure than before the measure (Supplementary Fig. 13).

CH+ chromophores

All CH chromophores identified in this study have $X_c \geq 2.5$, among which over 95% have $X_c \geq 2.7$ (Supplementary Fig. 15), suggesting they are likely polycyclic aromatic hydrocarbons (PAHs) that have been identified as important chromophores in WI-BrC fraction in ambient aerosols⁵³. In this study, a total of 564 and 512 CH+ chromophores were assigned in the WI-BrC fraction before and after the “coal-to-gas” measure, respectively. The corresponding intensity of most CH+ chromophores (>95%) was higher before the measure than after the measure, indicating that after the “coal-to-gas” conversion measure, the CH+ chromophores in atmospheric aerosols decreased significantly, which can be ascribed to the reduction of combustion emissions^{54,55}.

DISCUSSION

This study reveals obvious changes in the chemical composition of atmospheric BrC in Beijing during the heating period before and after the “coal-to-gas” conversion measure, providing new insights into the importance of coal combustion in the real world as a BrC source. After the measure, the number and intensity of WI-BrC chromophores decreased, while the number and intensity of HULIS-BrC chromophores increased. Besides, more highly

oxygenated chromophores were found in the HULIS-BrC fraction, and fewer low-oxygenated chromophores existed in the WI-BrC fraction after the measure than before the measure, likely due to the reduction in residential coal emissions as well as the change of atmospheric oxidative capacity. These results suggest that the impact of emission reduction measures on the chemical composition of BrC is complex, and more research is needed in the future. For example, some studies have shown that coatings of BrC on BC can enhance BC's light absorption^{56–58}; it is important to understand the influence of the “coal-to-gas” conversion measure on the mixing state of carbonaceous aerosol and thus the effects on radiative forcing. Besides, the enhancement of water-soluble BrC after the measure may lead to an increase of the aerosol and liquid water content and thus the formation of secondary BrC via aqueous photoreactions, which consequently affect the lifetime of BrC in the atmosphere^{59–61}. The changes in the chemical composition of BrC could also transform the size distribution of atmospheric particles, thereby affecting the light absorption and radiative forcing of atmospheric particles^{54,62,63}.

METHODS

Ambient samples

Daily ambient PM_{2.5} filter samples were collected from 17 January to 15 March in 2015 and 2019 on the rooftop (~20 m above the ground; 39.99°N, 116.32°E) of the National Center for Nanoscience and Technology in Beijing, China, which was surrounded by residential, traffic and commercial areas. Filter samples were collected on pre-baked (780 °C, 3 h) quartz-fiber filters (20.3 × 25.4 cm; Whatman, QM-A, Clifton, NJ, USA) using a high-volume PM_{2.5} sampler (1.05 m³ min⁻¹; Tisch, Cleveland, OH). After collection, the samples were wrapped in baked aluminum foils and stored in a freezer at -20 °C until further analysis.

Chemical analysis

The combined filter samples (3.526 cm² for each of the 6 high light absorption samples) were extracted for different organic carbon (OC) fractions. In order to get a more meaningful result, the selected samples all have light absorption coefficient (Abs) above the average value (average Abs at 365 nm (Abs₃₆₅) of 23.0 ± 14.2 and 10.0 ± 6.2 M m⁻¹ before and after “coal-to-gas” conversion measure, respectively), and the Abs₃₆₅ and OC concentration of selected samples were shown in Supplementary Table 2. The water-soluble fraction was extracted twice with 5 mL of ultrapure water (>18.2 MΩ cm) in an ultrasonic bath for 30 min. Then, the solution was filtered with a polyvinylidene fluoride (PVDF) syringe filter (Whatman, 0.45 μm; 3 mm) and treated following the protocol described by Lin et al.⁶⁴ to obtain HULIS fraction, which is the primary light absorption component of water-soluble BrC (WS-BrC)⁵³. The residual filter after water extraction was dried in a fume hood and further extracted twice with 5 mL methanol (HPLC grade, J.T. Baker, Phillipsburg, NJ, USA) in an ultrasonic bath for 30 min and filtered with a PTFE syringe filter for water-insoluble organic carbon (WISOC) fraction. The HULIS and WISOC fractions were concentrated to 300 μL for further analysis with an HPLC-PDA-HRMS. More details about HPLC-PDA-HRMS analysis were described elsewhere⁵³.

Data processing

Xcalibur 4.0 software (Thermo Scientific) was used to acquire raw data, and the open-source software toolbox MZmine version 2.52 (<http://mzmine.github.io/>) was used to perform peak deconvolution and chromatogram construction^{30,53}. The formula assignment was performed with the following constraints: C_{1–30}H_{0–60}O_{0–15}N_{0–3}S_{0–1}Na_{0–1} with a mass tolerance of ± 3 ppm for the ESI⁺ model and ± 2 ppm for the ESI⁻ model⁵³. The recognized formulas were restricted by

setting $0.3 \leq H/C \leq 3.0$, $O/C \leq 3.0$, $N/C \leq 0.5$, $S/C \leq 0.2$ to eliminate the chemically unreasonable formulas^{24,53}. Further, the compounds with $DBE/C \geq 0.5$ were considered candidates for BrC chromophores^{20,53}. The double-bond equivalent values of the neutral chemical formula of $C_cH_hO_oN_nS_sNa_x$ were calculated as $DBE = (2C + 2 - H + N)/2$, where C, H, N are the number of carbon, hydrogen, and nitrogen, respectively^{20,53}, and the aromaticity equivalent (Xc) was obtained using the equations: $Xc = [3(DBE - (mO + nS)) - 2]/[DBE - (mO + nS)]$, where m and n refer to the fraction of oxygen and sulfur atoms involved in the π -bound structure of a compound^{26,38}. In this study, $m = n = 0.5$ was employed for chromophores detected in ESI⁻ mode, and $m = n = 1$ was used for chromophores assigned in ESI⁺ mode³⁸. The neutral molecular formulas which did not conform to the nitrogen rule or with non-integer or negative DBE were excluded. All reported results have been corrected for blank. The peak intensity of the chromophores was used to compare their relative contents^{24,36,38,44}. It should be noted that different types of chromophores may exhibit distinct sensitivity in the mass spectrometer due to the differences in ionization and transmission efficiencies^{38,65}. Therefore, uncertainties may exist when comparing the peak intensity among chromophores. In this work, we assume that all chromophores have the same peak abundance response in the mass spectrometer.

DATA AVAILABILITY

Raw data used in this study are archived at the Institute of Earth Environment, Chinese Academy of Sciences, and are available on request by contacting the corresponding author (rujin.huang@ieecas.cn).

Received: 8 July 2022; Accepted: 9 March 2023;

Published online: 23 March 2023

REFERENCES

- Huang, R.-J. et al. High secondary aerosol contribution to particulate pollution during haze events in China. *Nature* **514**, 218–222 (2014).
- Burnett, R. et al. Global estimates of mortality associated with long-term exposure to outdoor fine particulate matter. *Proc. Natl Acad. Sci. USA* **115**, 9592–9597 (2018).
- Huang, R.-J. et al. Source-specific health risk analysis on particulate trace elements: coal combustion and traffic emission as major contributors in wintertime Beijing. *Environ. Sci. Technol.* **52**, 10967–10974 (2018).
- Bates, J. T. et al. Review of acellular assays of ambient particulate matter oxidative potential: Methods and relationships with composition, sources, and health effects. *Environ. Sci. Technol.* **53**, 4003–4019 (2019).
- Myhre, G. et al. Radiative forcing of the direct aerosol effect from AeroCom Phase II simulations. *Atmos. Chem. Phys.* **13**, 1853–1877 (2013).
- Schmale, J., Zieger, P. & Ekman, A. M. L. Aerosols in current and future Arctic climate. *Nat. Clim. Change* **11**, 95–105 (2021).
- Liu, P. et al. The contribution of residential coal combustion to atmospheric PM_{2.5} in northern China during winter. *Atmos. Chem. Phys.* **17**, 11503–11520 (2017).
- Huang, X. et al. Chemical characterization and source identification of PM_{2.5} at multiple sites in the Beijing–Tianjin–Hebei region, China. *Atmos. Chem. Phys.* **17**, 12941–12962 (2017).
- Huang, R.-J. et al. Primary emissions versus secondary formation of fine particulate matter in the most polluted city (Shijiazhuang) in North China. *Atmos. Chem. Phys.* **19**, 2283–2298 (2019).
- Yu, S. et al. Characteristics and oxidative potential of atmospheric PM_{2.5} in Beijing: source apportionment and seasonal variation. *Sci. Total Environ.* **650**, 277–287 (2019).
- Gu, Y. et al. Chemical nature and sources of fine particles in urban Beijing: seasonality and formation mechanisms. *Environ. Int.* **140**, 105732 (2020).
- Zhang, A. et al. Modeling the global radiative effect of brown carbon: a potentially larger heating source in the tropical free troposphere than black carbon. *Atmos. Chem. Phys.* **20**, 1901–1920 (2020).
- Jo, D. S., Park, R. J., Lee, S., Kim, S.-W. & Zhang, X. A global simulation of brown carbon: implications for photochemistry and direct radiative effect. *Atmos. Chem. Phys.* **16**, 3413–3432 (2016).
- Mok, J. et al. Impacts of brown carbon from biomass burning on surface UV and ozone photochemistry in the Amazon Basin. *Sci. Rep.* **6**, 36940 (2016).
- Zhang, Y. et al. Top-of-atmosphere radiative forcing affected by brown carbon in the upper troposphere. *Nat. Geosci.* **10**, 486–489 (2017).
- Zeng, L. et al. Global measurements of brown carbon and estimated direct radiative effects. *Geophys. Res. Lett.* **47**, e2020GL088747 (2020).
- Yan, C. et al. Important fossil source contribution to brown carbon in Beijing during winter. *Sci. Rep.* **7**, 43182 (2017).
- Xie, C. et al. Vertical characterization of aerosol optical properties and brown carbon in winter in urban Beijing, China. *Atmos. Chem. Phys.* **19**, 165–179 (2019).
- Ni, H. et al. Brown carbon in primary and aged coal combustion emission. *Environ. Sci. Technol.* **55**, 5701–5710 (2021).
- Lin, P., Fleming, L. T., Nizkorodov, S. A., Laskin, J. & Laskin, A. Comprehensive molecular characterization of atmospheric brown carbon by high resolution mass spectrometry with electrospray and atmospheric pressure photoionization. *Anal. Chem.* **90**, 12493–12502 (2018).
- Lobodin, V. V., Marshall, A. G. & Hsu, C. S. Compositional space boundaries for organic compounds. *Anal. Chem.* **84**, 3410–3416 (2012).
- Laskin, J. et al. Molecular selectivity of brown carbon chromophores. *Environ. Sci. Technol.* **48**, 12047–12055 (2014).
- West, C. P. et al. Molecular composition and optical properties of brown carbon generated by the ethane flame. *ACS Earth Space Chem.* **4**, 1090–1103 (2020).
- Lin, P., Rincon, A. G., Kalberer, M. & Yu, J. Z. Elemental composition of HULIS in the Pearl River Delta Region, China: results inferred from positive and negative electrospray high resolution mass spectrometric data. *Environ. Sci. Technol.* **46**, 7454–7462 (2012).
- Cech, N. B. & Enke, C. G. Practical implications of some recent studies in electrospray ionization fundamentals. *Mass Spectrom. Rev.* **20**, 362–387 (2001).
- Steimer, S. S. et al. Differences in the composition of organic aerosols between winter and summer in Beijing: a study by direct-infusion ultrahigh-resolution mass spectrometry. *Atmos. Chem. Phys.* **20**, 13303–13318 (2020).
- Jiang, B. et al. Molecular composition of urban organic aerosols on clear and hazy days in Beijing: a comparative study using FT-ICR MS. *Environ. Chem.* **13**, 888–901 (2016).
- Wang, X. et al. Chemical characteristics and brown carbon chromophores of atmospheric organic aerosols over the Yangtze River channel: a cruise campaign. *J. Geophys. Res.* **125**, e2020JD032497 (2020).
- Yan, C. et al. Molecular characterization of water-soluble brown carbon chromophores in Beijing, China. *J. Geophys. Res.* **125**, e2019JD032018 (2020).
- Fleming, L. T. et al. Molecular composition of particulate matter emissions from dung and brushwood burning household cookstoves in Haryana, India. *Atmos. Chem. Phys.* **18**, 2461–2480 (2018).
- Tang, J. et al. Molecular compositions and optical properties of dissolved brown carbon in biomass burning, coal combustion, and vehicle emission aerosols illuminated by excitation–emission matrix spectroscopy and Fourier transform ion cyclotron resonance mass spectrometry analysis. *Atmos. Chem. Phys.* **20**, 2513–2532 (2020).
- Walgraeve, C., Demeestere, K., Dewulf, J., Zimmermann, R. & van Langenhove, H. Oxygenated polycyclic aromatic hydrocarbons in atmospheric particulate matter: Molecular characterization and occurrence. *Atmos. Environ.* **44**, 1831–1846 (2010).
- Riva, M., Robinson, E. S., Perraudin, E., Donahue, N. M. & Villenave, E. Photochemical aging of secondary organic aerosols generated from the photooxidation of polycyclic aromatic hydrocarbons in the gas-phase. *Environ. Sci. Technol.* **49**, 5407–5416 (2015).
- Wang, X. et al. Chemical characteristics of organic aerosols in Shanghai: a study by ultrahigh-performance liquid chromatography coupled with orbitrap mass spectrometry. *J. Geophys. Res.* **122**, 11703–11722 (2017).
- Siemens, K. et al. Molecular analysis of secondary brown carbon produced from the photooxidation of naphthalene. *Environ. Sci. Technol.* **56**, 3340–3353 (2022).
- Song, J. et al. Molecular characterization of water- and methanol-soluble organic compounds emitted from residential coal combustion using ultrahigh-resolution electrospray ionization fourier transform ion cyclotron resonance mass spectrometry. *Environ. Sci. Technol.* **53**, 13607–13617 (2019).
- Zhao, R. et al. Light absorption properties and molecular compositions of water-soluble and methanol-soluble organic carbon emitted from wood pyrolysis and combustion. *Sci. Total Environ.* **809**, 151136 (2022).
- Wang, K. et al. Urban organic aerosol composition in eastern China differs from north to south: molecular insight from a liquid chromatography–mass spectrometry (Orbitrap) study. *Atmos. Chem. Phys.* **21**, 9089–9104 (2021).
- Lin, P. et al. Molecular chemistry of atmospheric brown carbon inferred from a nationwide biomass burning event. *Environ. Sci. Technol.* **51**, 11561–11570 (2017).
- Lim, Y. B., Kim, H., Kim, J. Y. & Turpin, B. J. Photochemical organonitrate formation in wet aerosols. *Atmos. Chem. Phys.* **16**, 12631–12647 (2016).
- Jang, K.-S. et al. Assessment of PM_{2.5}-bound nitrogen-containing organic compounds (NOCs) during winter at urban sites in China and Korea. *Environ. Pollut.* **265**, 114870 (2020).

42. Wang, Y. et al. The formation of nitro-aromatic compounds under high NO_x and anthropogenic VOC conditions in urban Beijing, China. *Atmos. Chem. Phys.* **19**, 7649–7665 (2019).
43. Laskin, A., Smith, J. S. & Laskin, J. Molecular characterization of nitrogen-containing organic compounds in biomass burning aerosols using high-resolution mass spectrometry. *Environ. Sci. Technol.* **43**, 3764–3771 (2009).
44. Wang, K., Zhang, Y., Huang, R.-J., Cao, J. & Hoffmann, T. UHPLC-Orbitrap mass spectrometric characterization of organic aerosol from a central European city (Mainz, Germany) and a Chinese megacity (Beijing). *Atmos. Environ.* **189**, 22–29 (2018).
45. Liu, S. et al. Enhancing effect of NO₂ on the formation of light-absorbing secondary organic aerosols from toluene photooxidation. *Sci. Total Environ.* **794**, 148714 (2021).
46. Jiang, H. et al. Factors influencing the molecular compositions and distributions of atmospheric nitrogen-containing compounds. *J. Geophys. Res. -Atmos.* **127**, e2021JD036284 (2022).
47. Wang, W. et al. Molecular characterization of organic aerosols in Taiyuan, China: Seasonal variation and source identification. *Sci. Total Environ.* **800**, 149419 (2021).
48. Song, J. et al. Molecular characterization of nitrogen-containing compounds in humic-like Substances emitted from biomass burning and coal combustion. *Environ. Sci. Technol.* **56**, 119–130 (2022).
49. Surratt, J. D. et al. Organosulfate formation in biogenic secondary organic aerosol. *J. Phys. Chem. A* **112**, 8345–8378 (2008).
50. Wang, X. K. et al. Molecular characterization of atmospheric particulate organosulfates in three megacities at the middle and lower reaches of the Yangtze River. *Atmos. Chem. Phys.* **16**, 2285–2298 (2016).
51. Breton, M. L. et al. Online gas- and particle-phase measurements of organosulfates, organosulfonates and nitrooxy organosulfates in Beijing utilizing a FIGAERO ToF-CIMS. *Atmos. Chem. Phys.* **18**, 10355–10371 (2018).
52. Kundu, S. et al. Evidence and quantitation of aromatic organosulfates in ambient aerosols in Lahore, Pakistan. *Atmos. Chem. Phys.* **13**, 4865–4875 (2013).
53. Huang, R.-J. et al. Water-insoluble organics dominate brown carbon in wintertime urban aerosol of china: chemical characteristics and optical properties. *Environ. Sci. Technol.* **54**, 7836–7847 (2020).
54. Chen, Q. et al. Size-resolved characterization of the chromophores in atmospheric particulate matter from a typical coal-burning city in China. *J. Geophys. Res.* **124**, 10546–10563 (2019).
55. Fleming, L. T. et al. Molecular composition and photochemical lifetimes of brown carbon chromophores in biomass burning organic aerosol. *Atmos. Chem. Phys.* **20**, 1105–1129 (2020).
56. Lack, D. A. & Cappa, C. D. Impact of brown and clear carbon on light absorption enhancement, single scatter albedo and absorption wavelength dependence of black carbon. *Atmos. Chem. Phys.* **10**, 4207–4220 (2010).
57. Cheng, Y. et al. Brown and black carbon in Beijing aerosol: implications for the effects of brown coating on light absorption by black carbon. *Sci. Total Environ.* **599**, 1047–1055 (2017).
58. Moschos, V. et al. Source-specific light absorption by carbonaceous components in the complex aerosol matrix from yearly filter-based measurements. *Atmos. Chem. Phys.* **21**, 12809–12833 (2021).
59. Zhao, R. et al. Photochemical processing of aqueous atmospheric brown carbon. *Atmos. Chem. Phys.* **15**, 6087–6100 (2015).
60. Smith, J. D., Kinney, H. & Anastasio, C. Phenolic carbonyls undergo rapid aqueous photodegradation to form low-volatility, light-absorbing products. *Atmos. Environ.* **126**, 36–44 (2016).
61. Hems, R. F. et al. Aqueous photoreactions of wood smoke brown carbon. *ACS Earth Sp. Chem.* **4**, 1149–1160 (2020).
62. Liu, J. et al. Size-resolved measurements of brown carbon in water and methanol extracts and estimates of their contribution to ambient fine-particle light absorption. *Atmos. Chem. Phys.* **13**, 12389–12404 (2013).
63. Wu, C. et al. The characteristics of atmospheric brown carbon in Xi'an, inland China: sources, size distributions and optical properties. *Atmos. Chem. Phys.* **20**, 2017–2030 (2020).
64. Lin, P., Engling, G. & Yu, J. Z. Humic-like substances in fresh emissions of rice straw burning and in ambient aerosols in the Pearl River Delta Region, China. *Atmos. Chem. Phys.* **10**, 6487–6500 (2010).
65. Krueve, A., Kaupmees, K., Liigand, J. & Leito, I. Negative electrospray ionization via deprotonation: predicting the ionization efficiency. *Anal. Chem.* **86**, 4822–4830 (2014).

ACKNOWLEDGEMENTS

This work was supported by the National Natural Science Foundation of China (NSFC) under Grant No. 41925015, the Key Research Program of Frontier Sciences from the Chinese Academy of Sciences (no. ZDBS-LY-DQC001), the Strategic Priority Research Program of the Chinese Academy of Sciences (no. XDB40000000), and SKLLQG (no. SKLLQGT1801).

AUTHOR CONTRIBUTIONS

Formal analysis, writing-original draft, W.Y., R.-J.H.; conceptualization, validation, supervision, project administration, funding acquisition R.-J.H.; writing-review & editing W.Y., R.-J.H., K.W., L.Y., T.W., Y.G., H.N., J.D., T.H.; data curation W.Y., R.-J.H., J.S., W.C., J.G.

COMPETING INTERESTS

The authors declare no competing interests.

ADDITIONAL INFORMATION

Supplementary information The online version contains supplementary material available at <https://doi.org/10.1038/s41612-023-00355-w>.

Correspondence and requests for materials should be addressed to Ru-Jin Huang.

Reprints and permission information is available at <http://www.nature.com/reprints>

Publisher's note Springer Nature remains neutral with regard to jurisdictional claims in published maps and institutional affiliations.



Open Access This article is licensed under a Creative Commons Attribution 4.0 International License, which permits use, sharing, adaptation, distribution and reproduction in any medium or format, as long as you give appropriate credit to the original author(s) and the source, provide a link to the Creative Commons license, and indicate if changes were made. The images or other third party material in this article are included in the article's Creative Commons license, unless indicated otherwise in a credit line to the material. If material is not included in the article's Creative Commons license and your intended use is not permitted by statutory regulation or exceeds the permitted use, you will need to obtain permission directly from the copyright holder. To view a copy of this license, visit <http://creativecommons.org/licenses/by/4.0/>.

© The Author(s) 2023